Chapter

In Silico Drug Design and Molecular Docking Studies of Some Quinolone Compound

Lucia Pintilie and Amalia Stefaniu

Abstract

Quinolones are an important class of heterocyclic compounds that possess interesting biological activities like antimicrobial, antitubercular, and antitumor. The objective of this study is to evaluate in *silico* the antitumoral and antimycobacterial activity of some quinolone derivatives by using CLC Drug Discovery Workbench Software. Docking studies were carried out for all ligands, and the docking scores were compared with the scores of standard drugs, topotecan and levofloxacin. The docking studies have been carried out to predict the most possible type of interaction, the binding affinities, and the orientations of the docked ligands at the active site of the target protein.

Keywords: molecular docking, quinolones, antimicrobial activity, antitumoral activity, antimycobacterial activity

1. Introduction

In medical practice, many quinolone derivatives with antimicrobial activity are used; some of these being considered by pharmacists as the primary drugs in human and veterinary anti-infectious therapy. Quinolones have a broad spectrum and a strong antibacterial activity [1, 2]. They are characterized by pharmacokinetics that allows their use in all localized infections. Recently, pharmacological studies have shown that quinolones also possess other biological activities: antitumor activity [3–6], antimycobaterial activity [7], antiviral activity on herpes virus, inhibiting neurovegetative diseases and ischemic infections, and food product storage (due to bactericidal properties). First antitumoral quinolone is Voreloxin: (+)-1,4-dihydro-7-(3S4S)-3-hydroxy-4-amino-1-pyrrolidinyl-4-oxo-1-(2-thiazolyl)-1.8-naphthyridine-3-carboxylic acid (**Figure 1**) [3]. Some quinolone derivatives (e.g., Moxifloxacin: 1-cyclopropyl-6-fluoro-7-((4aS,7aS)-hexahydro-1H-pyrrolo[3,4-b]pyridin-6(2H)-yl)-8-methoxy-4-oxo-1,4-dihydroquinoline-3-carboxylic acid-**Figure 2**) show activity against *Mycobacterium tuberculosis*, and these compounds are the first new antimycobacterial drugs to be available since the discovery of rifampin [8].

Lascufloxacin (AM-1977) (**Figure 3**) [9, 10] is a new 8-methoxy fluoroquinolone antibacterial agent with unique pharmacophores at the first and seventh positions of the quinolone rings. The oral and parenteral formulations have been developed for the treatment of community-acquired pneumonia and other respiratory tract infections in Japan. Lascufloxacin shows *in vitro* activity against various respiratory

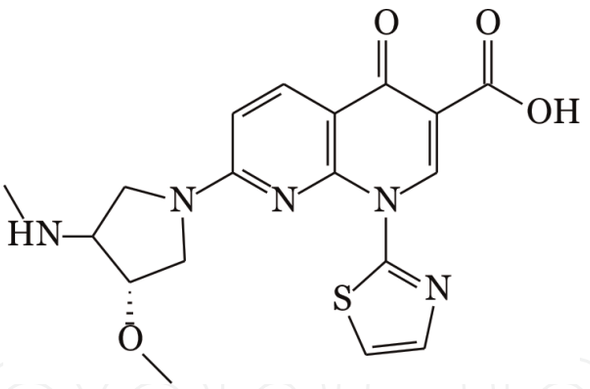

Figure 1.
Voreloxin.

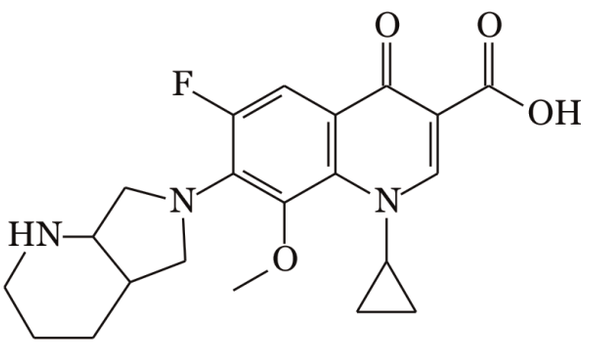

Figure 2.
Moxifloxacin.

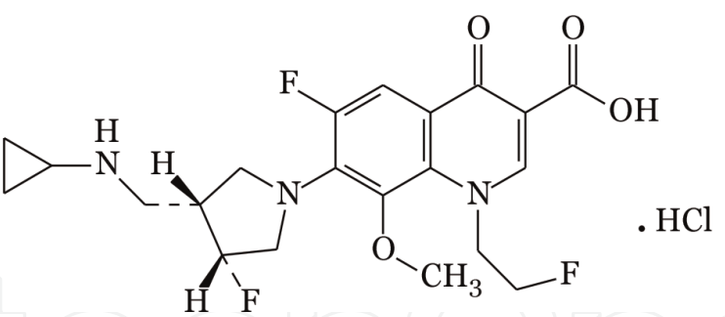

Figure 3.
Lascufloxacin.

pathogens, such as *Staphylococcus aureus*, *Streptococcus pneumoniae*, *Moraxella catarrhalis*, *Haemophilus influenzae,* and *Mycoplasma pneumoniae*.

Quinolones, considered to be "privileged building blocks," are obtained through simple and flexible synthesis methods and allow design and development of large libraries of bioactive molecules. A 2011 study on 21 antibiotics launched since 2000 has highlighted that the discovery and development of new antibiotics obtained through chemical synthesis is still topical. Of the nine antibiotics obtained by chemical synthesis, launched between 2000 and 2011, eight antibiotics belong to the class of fluoroquinolones [11]. New drugs introduced into medical therapies each year are privileged structures for specific biological targets. These new chemical entities provide a perspective on molecular recognition, serving as a basis for designing future new drugs. In 2016, 19 chemically synthesized drugs were approved [12], with the two drugs having the quinolone structure: nemonoxacin (**Figure 4**) and zabofloxacin (**Figure 5**).

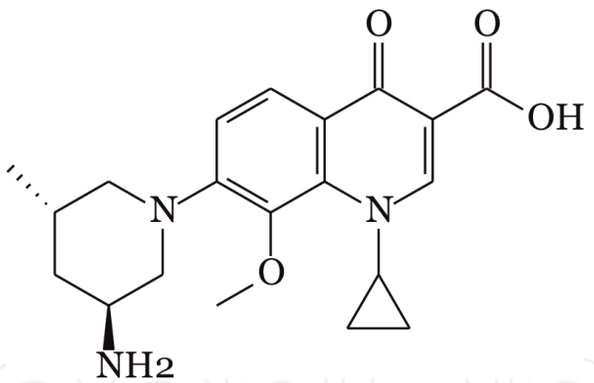

Figure 4.
Nemonoxacin (Taigexyn).

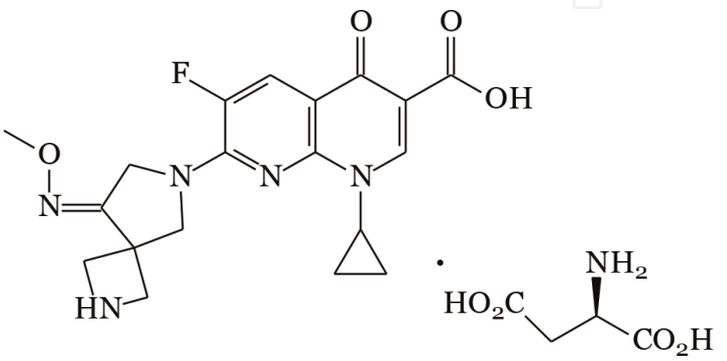

Figure 5.
Zabofloxacin D-aspartate.

The objective of this study is to evaluate "*in silico*" antitumoral and antimycobacterial activities of some quinolone derivatives by using CLC Drug Discovery Workbench Software [13]. Docking studies were conducted for all ligands, and the docking scores were compared with the scores of standard drugs, topotecan and levofloxacin.

2. Materials and methods

2.1 Structure and the synthesis pathway of the quinolone derivatives

In previous papers, we presented the synthesis of quinolone derivatives with antimicrobial activity [1, 2]. The results have revealed that the compounds represented in **Figure 6** have showed weak antibacterial activities against the tested strains. For this reason, we have initiated *in silico* drug design and molecular docking studies to predict anticancer and antitubercular activities targeting DNA-topoisomerase I and topoisomerase IV from *Klebsiella pneumoniae*, respectively.

We have performed molecular docking studies to see how the nature of substituents on the quinolone ring influences the anticancer and antitubercular activities targeting human DNA topoisomerase I and topoisomerase IV from *Klebsiella pneumoniae*, respectively. The studies have been realized with CLC Drug Discovery Workbench Software [13] in order to achieve accurate predictions on optimized conformations for both the quinolones (as ligands) and their target receptor proteins to form stable complexes.

The quinolone compounds have been synthesized by Gould-Jacobs cyclization process (**Figure 7**). Appropriate unsubstituted aniline (**1**) is reacted with diethyl

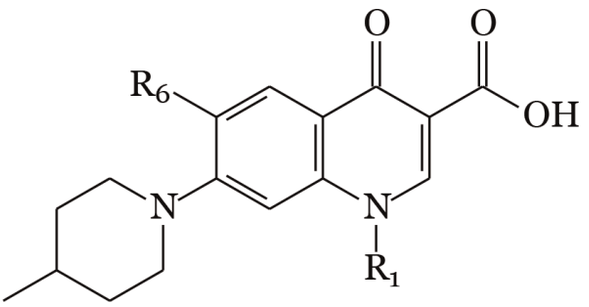

Figure 6.
General structure of the investigated quinolone compounds, where R_1 = allyl, iso*propyl, benzyl,* p*-nitro-phenyl,* p*-amino-phenyl and R_6 = F, Cl, H, CH_3.*

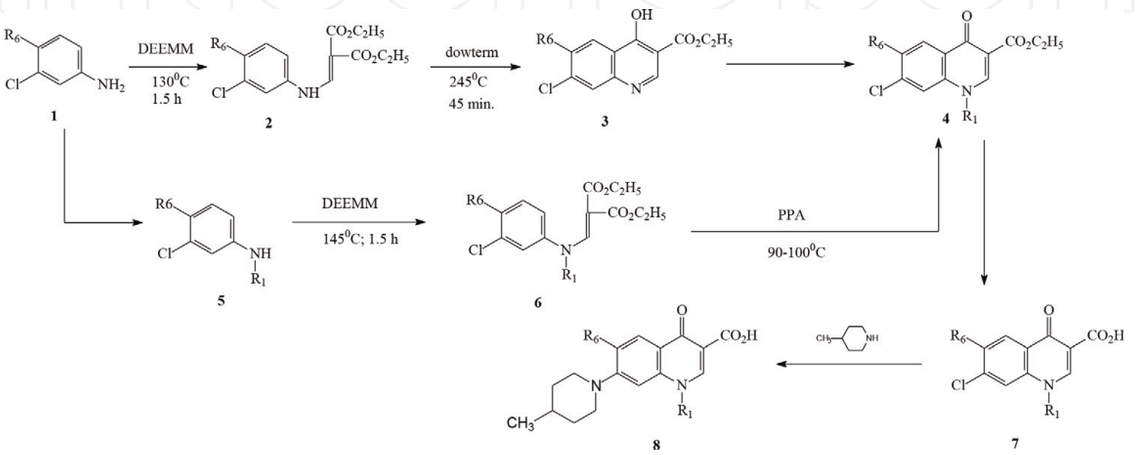

Figure 7.
The synthesis of the quinolone compound using Gould-Jacobs cyclization process.

ethoxymethylenemalonate (DEEMM) to produce the anilinomethylene malonate derivatives (**2**). A subsequent thermal process induces Gould-Jacobs cyclization to afford the corresponding 4-hydroxy-quinoline-3-carboxylate ethyl ester (**3**). The following operation is the alkylation/arylation of the quinolone compound (**4**), which is usually accomplished by reaction with allyl chloride, benzyl chloride, or *para* fluoronitrobenzene to produce the qinolone-3-carboxylate ester (**4**) (R_1 = allyl, benzyl, *para* nitrophenyl) [14–16, 19, 20]. The qinolone-3-carboxylate ester (**4**) (R_1 = *iso*propyl) was obtained by the reaction of the corresponding monosubstituted aniline (**5**) (R_1 = *iso*propyl) (the aniline (**5**) was obtained by reductive amination of acetone with sodium borohydride-acetic acid [14–16, 19] or triacetoxyborohydride [17, 18]) with DEEMM. A strong acid (such as polyphosphoric acid) is often needed to induce cyclization directly resulting in the formation of N-*iso*propyl-4-oxo-quinolone-3-carboxylate ester (**4**) (R_1 = *iso*propyl).

The final manipulation is the basic or acid hydrolysis that cleave the ester generating the biologically active free carboxylic acid (**7**) (R_1 = allyl, *iso*propyl, benzyl, *para* nitrophenyl). The displacement of 7-chloro group from the biologically active free carboxylic acid (**7**) with 4-methyl-piperidine yielded the compound (**8**) (R_1 = allyl, benzyl, *iso*propyl, *para* nitrophenyl) (**Table 1**). The quinolone compounds (**8**) (R_1 = *para* amino phenyl) (**Table 1**) have been synthesized by a common reduction of nitro group using sodium dithionite [20].

2.2 Ligand preparation

To achieve the docking studies, the quinolone derivatives (ligands) must be prepared to be imported in the molecular docking project. The ligands (**Table 1**)

Quinolone derivatives	2D structures	3D optimized structures
PQ4:1-allyl-6-fluoro-7-(4-methyl-piperidin-1-yl)-1,4-dihydro-4-oxo-quinolin-3-carboxylic acid [14] E: −1171.69431 au	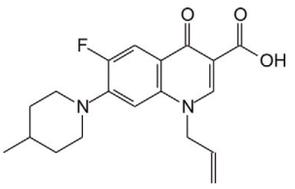	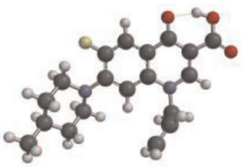
6ClPQ4:1-allyl-6-chloro-7-(4-methyl-piperidin-1-yl)-1,4-dihydro-4-oxo-quinolin-3-carboxylic acid [19] E: −1532.05076 au	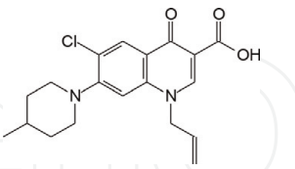	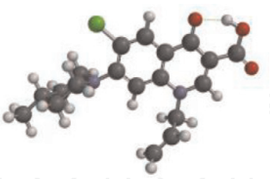
HPQ4:1-allyl-7-(4-methyl-piperidin-1-yl)-1,4-dihydro-4-oxo-quinolin-3-carboxylic acid [15] E: −1072.46696 au	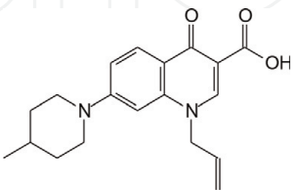	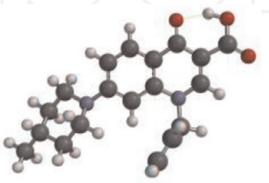
6MePQ4:1-allyl-6-methyl-7-(4-methyl-piperidin-1-yl)-1,4-dihydro-4-oxo-quinolin-3-carboxylic acid [16] E: −1111.77842 au	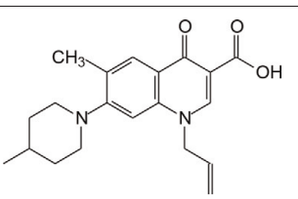	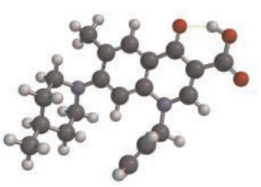
PQ12:1-*iso*propyl-6-fluoro-7-(4-methyl-piperidin-1-yl)-1,4-dihydro-4-oxo-quinolin-3-carboxylic acid [14] E: −1172.93189 au	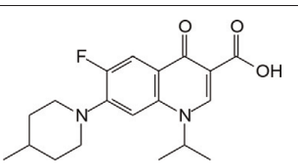	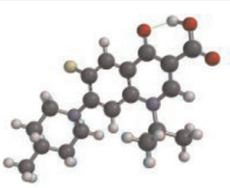
6ClPQ12:1-*iso*propyl-6-chloro-7-(4-methyl-piperidin-1-yl)-1,4-dihydro-4-oxo-quinolin-3-carboxylic acid [19] E: −1533.28880 au	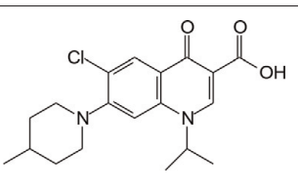	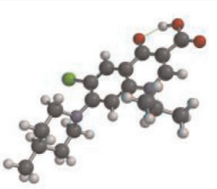
HPQ12:1-*iso*propyl-7-(4-methyl-piperidin-1-yl)-1,4-dihydro-4-oxo-quinolin-3-carboxylic acid [15] E: −1073.70428 au	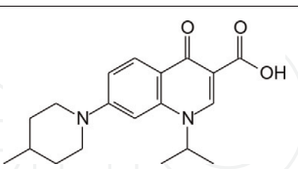	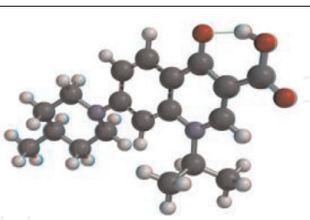
6MePQ12:1-*iso*propyl-6-methyl-7-(4-methyl-piperidin-1-yl)-1,4-dihydro-4-oxo-quinolin-3-carboxylic acid [16] E: −1113.01581 au	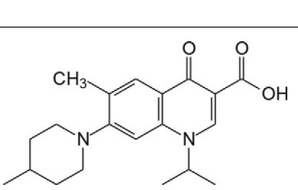	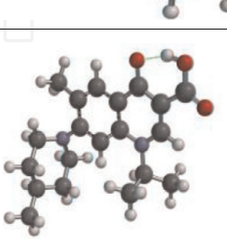
PQ11:1-benzyl-6-fluoro-7-(4-methyl-piperidin-1-yl)-1,4-dihydro-4-oxo-quinolin-3-carboxylic acid [14] E: −1325.35417 au	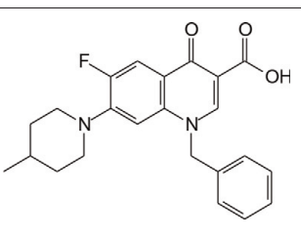	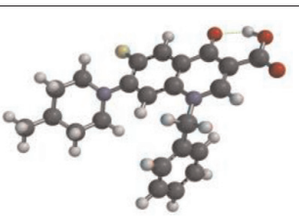

Quinolone derivatives	2D structures	3D optimized structures
6ClPQ11:1-benzyl-6-chloro-7-(4-methyl-piperidin-1-yl)-1,4-dihydro-4-oxo-quinolin-3-carboxylic acid [19] E: −1685.71018 au	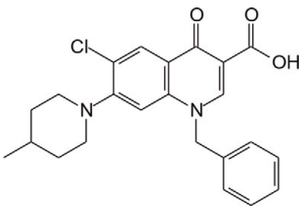	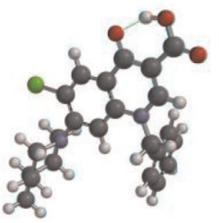
HPQ11:1-benzyl-7-(4-methyl-piperidin-1-yl)-1,4-dihydro-4-oxo-quinolin-3-carboxylic acid [15] E: −1226.12649 au	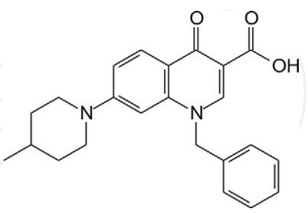	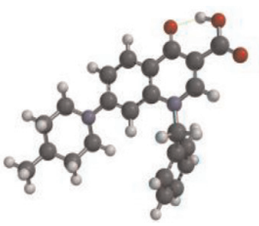
6MePQ11:1-benzyl-6-methyl-7-(4-methyl-piperidin-1-yl)-1,4-dihydro-4-oxo-quinolin-3-carboxylic acid [16] E: −1265.46016 au	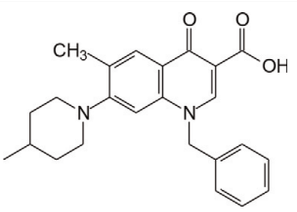	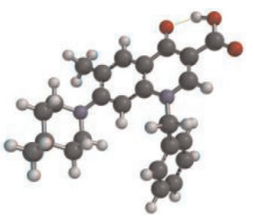
PQ13:1-(*p*-nitro-phenyl)-6-fluoro-7-(4-methyl-piperidin-1-yl)-1,4-dihydro-4-oxo-quinolin-3-carboxylic acid [20] E: −1490.53723 au	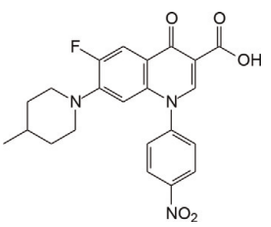	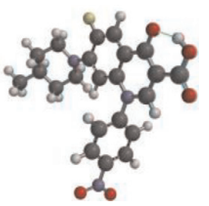
6ClPQ13:1-(*p*-nitro-phenyl)-6-chloro-7-(4-methyl-piperidin-1-yl)-1,4-dihydro-4-oxo-quinolin-3-carboxylic acid [20] E: −1850.89287 au	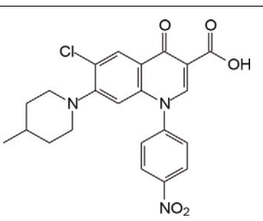	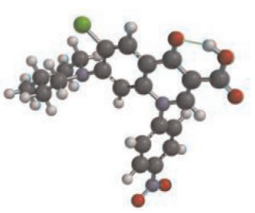
HPQ13:1-(*p*-nitro-phenyl)-7-(4-methyl-piperidin-1-yl)-1,4-dihydro-4-oxo-quinolin-3-carboxylic acid E: −1391.31010 au	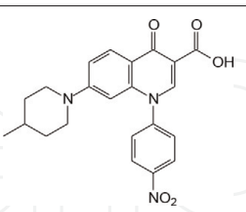	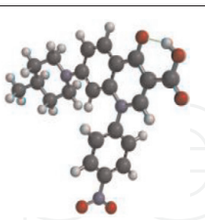
6MePQ13:1-(*p*-nitro-phenyl)-6-methyl-7-(4-methyl-piperidin-1-yl)-1,4-dihydro-4-oxo-quinolin-3-carboxylic acid [20] E: −430.62213 au	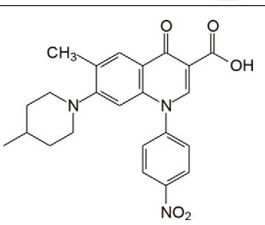	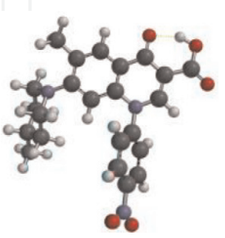
APQ13:1-(*p*-amino-phenyl)-6-fluoro-7-(4-methyl-piperidin-1-yl)-1,4-dihydro-4-oxo-quinolin-3-carboxylic acid [20] E: −1341.39572 au	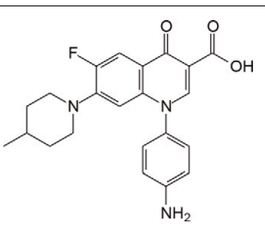	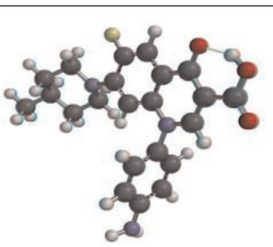

Quinolone derivatives	2D structures	3D optimized structures
A6ClPQ13: 1-(*p*-amino-phenyl)-6-chloro-7-(4-methyl-piperidin-1-yl)-1,4-dihydro-4-oxo-quinolin-3-carboxylic acid E: −1701.75238 au	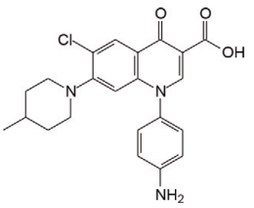	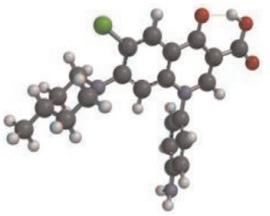
AHPQ13:1-(*p*-amino-phenyl)-7-(4-methyl-piperidin-1-yl)-1,4-dihydro-4-oxo-quinolin-3-carboxylic acid E: −1242.16807 au	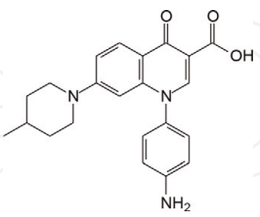	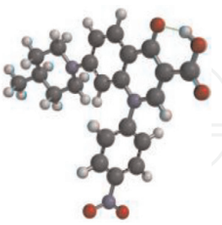
A6MePQ13:1-(*p*-amino-phenyl)-6-methyl-7-(4-methyl-piperidin-1-yl)-1,4-dihydro-4-oxo-quinolin-3-carboxylic acid [20] E: −1281.47987 au	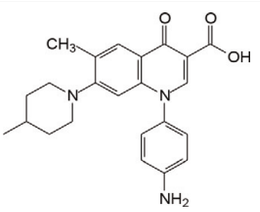	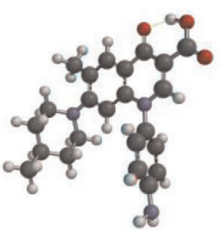

E = energy and au = atomic units.

Table 1.
The 2D and 3D structures of the quinolone compounds.

have been prepared using SPARTAN'14 software package [21] according to the protocol described in our previous work [22]. The DFT/B3LYP/6-31 G* level of basis set has been used for the computation of molecular structure, vibrational frequencies, and energies of optimized structures.

Some chemical properties, highest occupied molecular orbital (HOMO) and lowest unoccupied molecular orbital (LUMO) energy values, HOMO and LUMO orbital coefficient distribution, molecular dipole moment, polar surface area (PSA) (a descriptor that has been shown to correlate well with passive molecular transport through membranes, therefore, allows the prediction of transport properties of the drugs), the ovality, polarizability (useful to predict the interactions between non-polar atoms or groups and other electrically charged species, such as ions and polar molecules having a strong dipole moment), and the octanol water partition coefficient (log P) have been calculated (**Table 2**).

2.3 Docking studies

The docking protocol was performed according to the CLC Drug Discovery Workbench Software and was described in a previous paper [22]. The docking scores and hydrogen bonds formed with the amino acids from group interaction atoms were used to predict the binding modes, the binding affinities, and the orientation of the docked quinolone derivatives in the active site of the target proteins.

2.3.1 Docking evaluation against human DNA topoisomerase

Docking studies have been carried out in order to achieve accurate predictions on the optimized conformations for both the quinolone derivatives (as ligands) and

Compounds	Molecular properties									
	Dipole moment (Debye)	E HOMO (eV)	E LUMO (eV)	HOMO-LUMO GAP	Polarizability (10^{-30} m^3)	PSA (Å^2)	Ovality	Log P	HBA count	HBD count
PQ4	11.42	−5.88	−1.62	4.28	68.31	44.205	1.51	2.92	1	4
6ClPQ4	9.50	−6.24	−1.91	4.33	69.10	44.864	1.52	3.32	1	4
HPQ4	11.77	−5.85	−1.47	4.38	67.89	44.618	1.50	2.76	1	4
6MePQ4	11.65	−5.77	−1.43	4.34	69.36	44.396	1.51	3.35	1	4
PQ11	11.37	−5.88	−1.62	4.26	72.46	44.195	1.55	4.44	1	4
6ClPQ11	9.67	−6.18	−1.89	4.29	73.27	44.610	1.57	4.84	1	4
HPQ11	11.82	−5.82	−1.46	4.36	72.05	44.426	1.54	4.29	1	4
6MePQ11	11.78	−5.74	−1.40	4.34	73.50	44.271	1.55	3.38	1	4
PQ12	11.19	−5.94	−1.62	4.32	68.57	44.362	1.51	3.37	1	4
6ClPQ12	9.55	−6.18	−1.86	4.32	69.36	44.844	1.52	3.77	1	4
HPQ12	11.68	−5.88	−1.44	4.44	68.15	44.658	1.50	3.21	1	4
6MePQ12	11.16	−5.78	−1.38	4.40	69.64	44.246	1.50	3.70	1	4
PQ13	9.37	−6.03	−3.08	2.95	73.03	82.971	1.57	0.10	1	7
6ClPQ13	6.99	−6.37	−3.13	3.24	73.76	83.732	1.58	0.50	1	7
HPQ13	10.10	−6.06	−3.01	3.05	72.60	83.520	1.56	−0.06	1	7
6MePQ13	9.78	−5.98	−3.01	2.97	74.07	83.336	1.57	0.43	1	7
APQ13	13.57	−5.81	−1.49	4.32	71.82	61.120	1.56	2.75	2	5
6ClAPQ13	12.11	−6.11	−1.74	4.37	72.62	69.491	1.58	3.15	2	5
HAPQ13	13.91	−5.76	−1.32	4.44	71.41	69.419	1.55	2.59	2	5

Table 2.
Molecular properties for CPK model computations for quinolone compounds.

protein target to form a stable complex. All of the investigated compounds have been docked on the crystal structure of human DNA topoisomerase I (PDB ID: 1K4T) [23]. Binding site and docking pose of the co-crystallized topotecan (TTC), interacting with amino acid residues of the active site, are shown in **Figure 8a**. The TTC was taken as reference ligand to compare the docking results of quinolone derivatives. The docking score, the interacting group, and hydrogen bonds formed with the group interaction atoms of the corresponding amino acids are shown in **Table 3**. Interactions of quinolone derivatives PQ11 (score: −63.31 and RMSD: 0.12), 6ClPQ11 (score: −62.95 and RMSD: 0.08), HPQ11 (score: −62.77 and RMSD: 0.06), 6MePQ11(score: −62.48 and RMSD: 0.01), and 6MePQ13 (score: −61.22 and RMSD: 0.04) showed better docking score than that of co-crystalized TTC (score: −59.15 and RMSD: 0.14) as shown in **Figures 8b–11a**. The most active compound, 6ClPQ11, was predicted to have a significant docking score (−63.31) and forms one hydrogen bond with GLU 418 (bond length – 2.961 Å) (**Figure 9a**). Docking poses of all quinolone derivatives in the ligand binding site of human DNA topoisomerase I are shown in **Figure 11b**.

2.3.2 Docking evaluation against topoisomerase IV from Klebsiella pneumoniae

Docking studies have been carried out in order to obtain optimized docking conformations of the investigated quinolone derivatives on the crystal structure of topoisomerase IV (PDB ID: 5EIX) from *Klebsiella pneumoniae* [24]. The binding site and docking pose of the co-crystallized levofloxacin (LFX) ligand, interacting with amino acid residues of the ligand binding site of topoisomerase IV from *Klebsiella pneumoniae*, are shown in **Figure 12a**. The levofloxacin was taken as reference ligand to compare the docking results of quinolone derivatives. The docking score, the interacting group, and hydrogen bonds formed with the group interaction atoms of the corresponding amino acids are shown in **Table 4**. Interactions of quinolone derivatives PQ4 (score: −43.98 and RMSD: 0.05), 6ClPQ4 (score: −41.12 and RMSD: 0.25), PQ11 (score: −48.32 and RMSD: 0.10), HPQ11 (score: 49.57 and RMSD: 0.11), PQ12 (score: −42.76 and RMSD: 0.18), and APQ13 (score: −42.96 and RMSD: 0.32) showed better docking score than that of co-crystalized LFX (score: 37.26 and RMSD: 0.02) as shown in **Figures 12b–15a**. The most active compound,

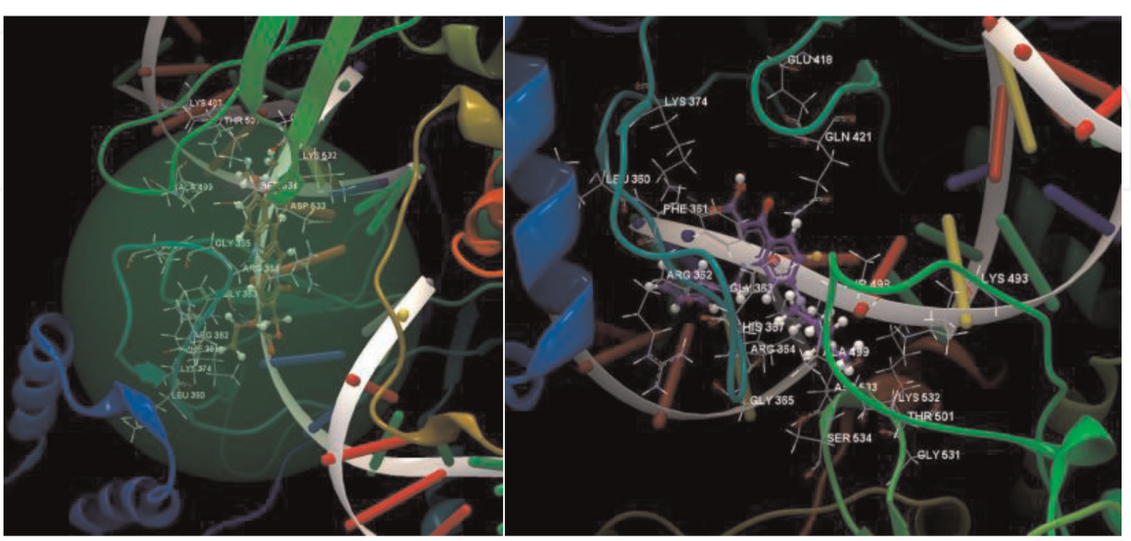

Figure 8.
(a) Binding site and docking pose of the co-crystallized TTC ligand interacting with the amino acid residues of the ligand binding site of human DNA topoisomerase I. (b) Docking pose of the PQ11 ligand interacting with the amino acid residues of the ligand binding site of human DNA topoisomerase I.

Ligand	Score/ RMSD (Å)	Group interaction/hydrogen bond	Bond length (Å)
TTC D-990	−59.15/ 0.14	LYS 493, THR 501, LYS 532, GLY 531, ALA 499, THR 498, SER 534, ASP 533, GLY 365, ARG 364, HIS 367, GLY 363, ARG 362, PHE 361, LYS 374, and LEU 360	
		O sp^3 from TTC– N sp^2 from ASP 533	3.065
		O sp^3 from TTC– O sp^3 from THR 501	3.166
		N sp^2 from TTC– N sp^2 from ARG 364	3.353
		O sp^3 from TTC– O sp^2 from GLY 363	3.112
		O sp^3 from TTC– N sp^2 from GLY 363	3.038
PQ4	−55.35/ 0.07	GLU 418, GLN 421, LYS 374, THR 498, PHE 361, GLY 363, HIS 367, ARG 364, ARG 362, GLY 365, SER 534, ASP 533, ALA 499, GLY 531, THR 501, ASP 500, and LYS 532	
		O sp^3 from CO_2H(OH)-N sp^3 from LYS 374	3.124
6ClPQ4	−55.81/ 0.12	LYS 425, TRP 416, ARG 364, GLY 363, ILE 377, ARG 362, PHE 361, LYS 374, ARG 375, LEU 360, MET 263, ILE 420, ASN 419, GLN 421, and GLU 418	
		O sp^3 from CO_2H(CO)-N sp^2 from ARG 364	3.056
		O sp^3 from CO_2H (OH)-O sp^2 from GLY 363	2.808
		O sp^2 from CO-N sp^2 from ARG 364	3.009
HPQ4	−56.08/ 0.10	ARG 364, LYS 425, GLY 363, ARG 362, GLN 421, GLU 418, PHE 361, ILE 420, ASN 118, LYS 374, ARG 375, ILE 377, LEU 360, and MET 263	
		O sp^3 from CO_2H(CO)-N sp^2 from ARG 364	2.782
		O sp^2 from CO-N sp^2 from ARG 364	2.887
6MePQ4	−55.52/ 0.10	GLU 418, GLN 421, LYS 374, THR 498, PHE 361, GLY 363, HIS 367, ARG 364, ARG 362, GLY 365, SER 534, ASP 533, ALA 499, GLY 531, THR 501, and LYS 532	
		O sp^3 from CO_2H (OH)-N sp^3 from LYS 374	3.040
PQ11	−62.95/ 0.08	GLU 418, GLN 421, LYS 374, LEU 360, THR 498, PHE 361, GLY 363, HIS 367, ARG 364, ARG 362, LYS 493, GLY 365, SER 534, ASP 533, ALA 499, GLY 531, THR 501, and LYS 532	
		O sp^3 from CO_2H (OH)-N sp^3 from LYS 374	3.214
6ClPQ11	−63.31/ 0.12	SER 423, LYS 425, GLN 421, GLU 418, ILE 420, LYS 374, LYS 493, THR 498, LYS 532, GLY 531, THR 501, ASP 533, ALA 499, SER 534, ARG 364, GLY 365, GLY 363, HIS 367, ARG 362, PHE 361, and LEU 360	
		O sp^3 from CO_2H(OH)-O sp^2 from GLU 418	2.961
HPQ11	−62.77/ 0.06	SER 423, LYS 425, GLN 421, GLU 418, ILE 420, LYS 374, LYS 493, THR 498, LYS 532, GLY 531, THR 501, ASP 533, ALA 499, SER 534, ARG 364, GLY 365, GLY 363, HIS 367, ARG 362, PHE 361, and LEU 360	
		O sp^2 from CO_2H(OH)-O sp^2 from ASP 533	3.144
		O sp^3 from CO_2H(CO)-N sp^2 from ARG 364	3.111
		O sp^3 from CO_2H(CO)-N sp^2 from ARG 364	2.748
6MePQ11	−62.48/ 0.01	GLU 418, GLN 421, LYS 374, THR 498, PHE 361, GLY 363, HIS 367, ARG 364, ARG 362, LYS 493, GLY 365, SER 534, ASP 533, ALA 499, GLY 531, THR 501, and LYS 532	
		O sp^3 from CO_2H (OH)-N sp^3 from LYS 374	3.042

Ligand	Score/ RMSD (Å)	Group interaction/hydrogen bond	Bond length (Å)
PQ12	−52.44/ 0.06	GLU 418, GLN 421, LYS 374, THR 498, PHE 361, GLY 363, HIS 367, ARG 364, ARG 362, LYS 493, GLY 365, SER 534, ASP 533, ALA 499, GLY 531, THR 501, and LYS 532	
		O sp^3 from CO_2H(OH)-N sp^3 from LYS 374	3.155
6ClPQ12	−50.48/ 0.29	GLU 418, GLN 421, GLU 356, LYS 374, THR 498, PHE 361, GLY 363, HIS 367, ARG 364, ARG 362, LYS 493, GLY 365, SER 534, ASP 533, ALA 499, GLY 531, THR 501, and LYS 532	
		O sp^3 from CO_2H(OH)-N sp^3 from LYS 374	3.059
		O sp^3 from CO_2H(CO)-N sp^3 from LYS 374	3.068
HPQ12	−51.36/ 0.37	GLU 418, GLN 421, LYS 425, SER 423, LYS 374, THR 498, PHE 361, GLY 363, HIS 367, ARG 364, LYS 493, GLY 365, ILE 420, SER 534, ASP 533, ALA 499, GLY 531, THR 501, and LYS 532	
		O sp^3 from CO_2H(OH)-N sp^3 from LYS 374	3.112
6MePQ12	−52.57/ 0.03	GLU 418, GLN 421, LYS 374, THR 498, PHE 361, ARG 362, GLY 363, HIS 367, ARG 364, LYS 493, GLY 365, SER 534, ASP 533, ALA 499, GLY 531, THR 501, and LYS 532	
		O sp^3 from CO_2H(OH)-N sp^3 from LYS 374	3.046
PQ13	−57.18/ 0.06	LYS 425, GLU 418, GLN 421, LYS 374, THR 498, PHE 361, ARG 362, GLY 363, HIS 367, ARG 364, LYS 493, LEU 360, GLY 365, SER 534, ASP 533, ALA 499, GLY 531, THR 501, and LYS 532	
		O sp^3 from CO_2H(OH)-N sp^3 from LYS 374	3.032
6ClPQ13	−58.51/ 0.09	GLU 418, GLN 421, LYS 374, THR 498, PHE 361, ARG 362, GLY 363, HIS 367, ARG 364, LYS 493, GLY 365, SER 534, ASP 533, ALA 499, GLY 531, THR 501, and LYS 532	
		O sp^3 from CO_2H(OH)-N sp^3 from LYS 374	3.099
HPQ13	−58.40/ 0.05	ARG 364, LYS 425, GLY 363, ARG 362, TYR 268, GLN 421, GLU 418, PHE 361, ILE 420, ASN 419, LYS 374, ARG 375, ILE 377, LEU 360, MET 263, SER 423, and TRP 416	2.989
		O sp^2 from CO_2H(CO)-N sp^3 from LYS 425	
		O sp^3 from CO_2H (CO-O sp^3 from SER 423	3.059
		O sp^2 from NO_2-N sp^2 from ASN 419	2.969
6MePQ13	−61.22/ 0.04	LYS 425, ARG 364, GLY 365, ASP 533, SER 531, THR 501, ARG 362, PHE 361, LYS 374, LYS 532, GLY 531, ALA 499, HIS 367, THR 498, LYS 493, SER 423, GLN 421, and GLU 418	
		O sp^3 from CO_2H(OH)-O sp^2 from GLU 418	2.978
APQ13	−60.00/ 0.06	GLU 418, LYS 425, GLN 421, LYS 374, THR 498, PHE 361, ARG 362, GLY 363, HIS 367, ARG 364, GLY 365, SER 534, ASP 533, ALA 499, GLY 531, THR 501, and LYS 532	
		O sp^3 from CO_2H(OH)-N sp^3 from LYS 374	3.008
6ClAPQ13	−57.07/ 0.64	LYS 425, ARG 364, GLU 356, GLY 365, ASP 533, GLY 531, THR 501, ARG 362, GLY 363, PHE 361, LYS 374, LYS 532, ALA 499, HIS 367, LYS 493, SER 534, GLN 421, and GLU 41	
		O sp^3 from CO_2H(OH)-N sp^3 from LYS 374	2.934
HAPQ13	−58.14/ 0.07	SER 423, LYS 425, GLN 421, GLU 418, ILE 420, ASN 419, LYS 374, ARG 364, GLY 363, ARG 362, PHE 361, ILE 377, ARG 375, LEU 360, and MET 263	
		O sp^2 from CO_2H(CO)-O sp^3 from LYS 425	2.874

Ligand	Score/ RMSD (Å)	Group interaction/hydrogen bond	Bond length (Å)
		O sp^3 from $CO_2H(CO)$-O sp^3 from SER 423	2.994
6MeAPQ13	−56.87/ 0.13	LYS 425, ARG 364, GLY 365, ASP 533, GLY 531, THR 501, ARG 362, GLY 363, THR 498, PHE 361, LYS 374, LYS 532, ALA 499, HIS 367, LYS 493, SER 534, GLN 421, and GLU 418	
		O sp^2 from $CO_2H(CO)$-N sp^3 from LYS 374	3.097

Table 3.
List of docking interactions between the ligand molecules and human DNA topoisomerase I using CLC Drug Discovery Workbench Software.

Figure 9.
(a) Docking pose of 6ClPQ 11 ligand interacting with amino acid residues of the ligand binding site of human DNA topoisomerase I. (b) Docking pose of HPQ11 ligand interacting with amino acid residues of the ligand binding site of human DNA topoisomerase I.

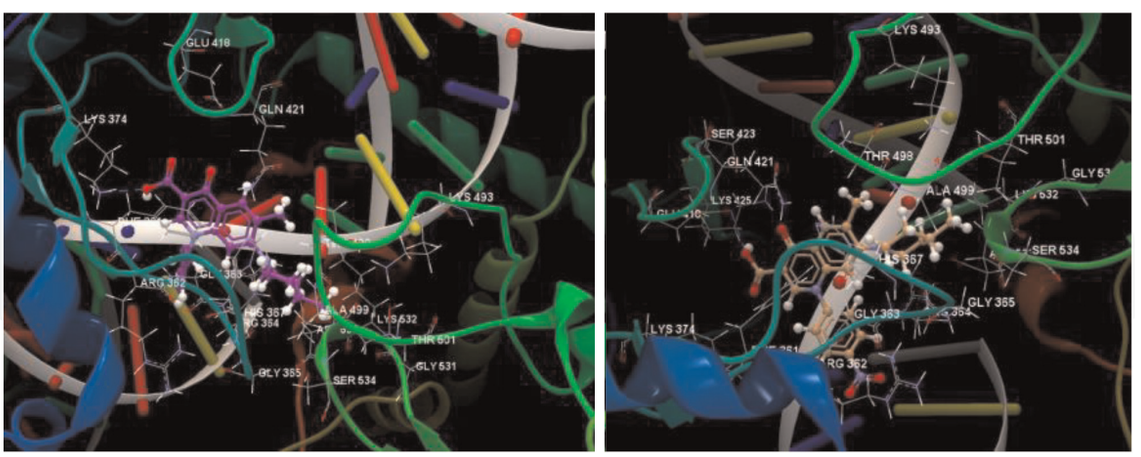

Figure 10.
(a) Docking pose of 6MePQ11 ligand interacting with amino acid residues of the ligand binding site of human DNA topoisomerase I. (b) Docking pose of 6MePQ13 ligand interacting with amino acid residues of the ligand binding site of human DNA topoisomerase I.

HPQ11, was predicted to have a significant docking score (−49.57) and forms one hydrogen bond with ASP95 (bond length – 3.081 Å) (**Figure 14a**). Docking poses of all quinolone derivatives in the ligand binding site of topoisomerase IV from *Klebsiella pneumoniae* are shown in **Figure 15b**.

Figure 11.
(a) Docking pose of APQ13 ligand interacting with amino acid residues of the ligand binding site of human DNA topoisomerase I. (b) Overlay of docking poses of all ligands interacting with amino acid residues of the ligand binding site of human DNA topoisomerase I.

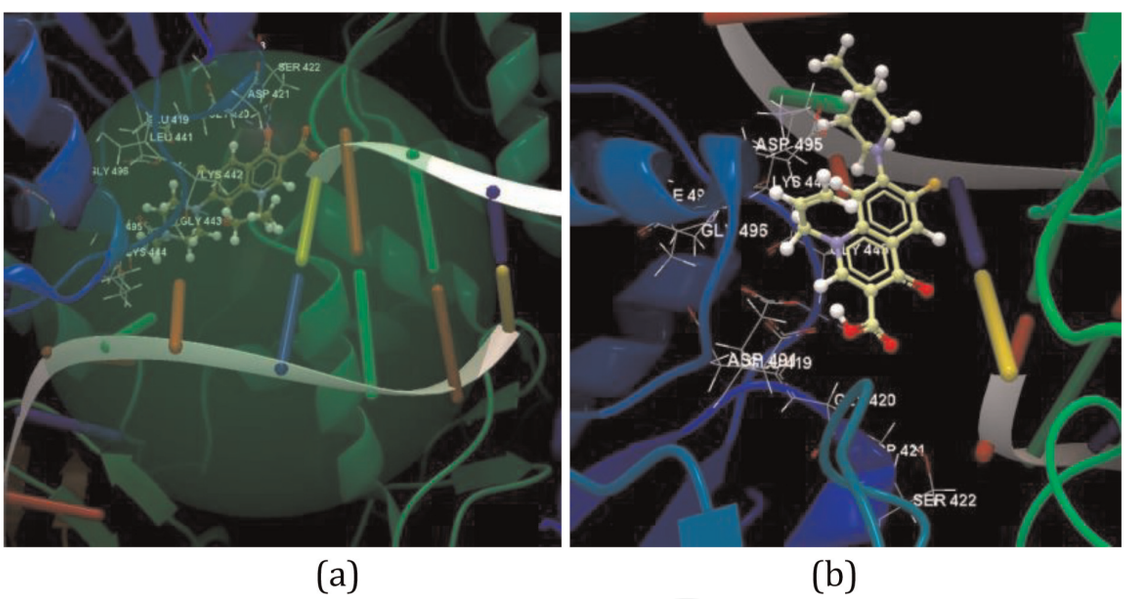

Figure 12.
(a) Binding site and docking pose of the co-crystallized LFX ligand interacting with the amino acid residues of ligand binding site of the topoisomerase IV. (b) Docking pose of the PQ4 ligand interacting with the amino acid residues of ligand binding site of the topoisomerase IV.

Important molecular properties of the investigated compounds, e.g., molecular weight, flexible bonds, the number of hydrogen bond donors, the number of hydrogen bond acceptors, and log P, have been calculated. These parameters can be used to evaluate whether a molecule has properties that would make it a likely orally active drug, according to the Lipinski's rule of five [22]. The number of violations of the Lipinski rules allows to evaluate drug likeness for a molecule (**Table 5**).

3. Results and discussions

All of the investigated compounds have been docked on human DNA topoisomerase (PDB ID: 1K4T) and topoisomerase IV (PDB ID: 5EIX) from *Klebsiella*

Ligand	Score/ RMSD (Å)	Group interaction/hydrogen bond	Bond length (Å)
LFX	−37.26/0.02	SER 422, ALA 423, ASP 421, GLY 420, LYS 442, LEU 441, GLY 443, GLU 419, LYS 444, ILE 499, GLY 496, and ASP 495	
		O sp^2 from CO-O sp^3 from SER 422	2.590
		O sp^2 from CO-N sp^2 from SER 422	2.856
		O sp^2 from CO-N sp^2 from ASP 421	3.098
		O $sp^3$from LVF-N sp^2 from GLY 443	3.344
PQ4	−43.98/0.05	SER 422, ASP 421, GLY 420, GLY 443, GLU 419, ASP 491, LYS 444, ILE 499, GLY 496, and ASP 495	
		O sp^2 from CO_2H(OH)-O sp^3 from GLU 419	2.702
6ClPQ4	−41.12/0.25	SER 422, ALA 423, ASP 421, GLY 420, LYS 499, LEU 441, GLY 443, GLU 419, ASP 491, ASP 493, LYS 444, ILE 499, GLY 496, and ASP 495	
		O sp^2 from CO-O sp^3 from SER 422	2.870
		O sp^2 from CO-N sp^2 from SER 422	3.162
HPQ4	−40.60/0.20	SER 422, ASP 421, GLY 420, GLY 443, GLU 419, ASP 491, LYS 444, ILE 499, GLY 496, and ASP 495	
		O sp^2 from CO_2H(OH)-O sp^3 from GLU 419	2.880
6MePQ4	−35.70/0.36	SER 422, ASP 421, GLY 420, GLY 443, GLU 419, ASP 491, LYS 444, ILE 499, GLY 496, and ASP 495	
		O sp^2 from CO_2 H(OH)-O sp^3 from GLU 419	2.911
PQ11	−48.32/0.10	LYS 444, ILE 499, ASP 495, ASP 493, GLY 443, LEU 441, GLU 419, ASP 491, GLY 420, LYS 442, ASP 421, LEU 567, ALA, 423, SER 422, and GLY 568	
		O sp^2 from CO_2H(OH)-O sp^2 from ASP 491	2.974
		O sp^2 from CO_2H (OH)-O sp^2 from GLU 419	2.606
		O sp^2 from CO-O sp^3 from SER 422	2.650
6ClPQ11	−41.14/0.28	SER 422, ASP 421, GLY 420, LYS 442, LEU 441, GLY 443, GLU 419, LYS 444, ILE 499, GLY 496, and ASP 495	
		O sp^2 from CO_2H(CO)-N sp^2 from ASP 421	3.062
HPQ11	−49.57/0.11	HIS 1077, ASP 421, GLY 420, ASP 493, LYS 442, LEU 441, GLU 419, GLY 443, LYS 444, ILE 499, ILE 445, ASP 495, and ARG 1029	
		O sp^2 from CO_2H(OH)-N sp^2 from ASP 495	3.081
6MePQ11	−39.64/0.18	SER 422, HIS 1077 ASP 421, GLY 420, ASP 491, ASP 493, LYS 442, LEU 441, GLU 419, GLY 443, LYS 444, ILE 499, ASP 495, ARG 1029, and ILE 445	
		O sp^2 from CO_2H (OH)-N sp^2 from ASP 495	3.088
PQ12	−42.76/0.18	HIS 1077, GLY 420, ASP 493, LYS 442, LEU 441, GLU 419, GLY 443, LYS 444, ILE 499, ILE 445, ASP 495, ASP 491, ARG 1029, and GLY 496	
		O sp^2 from CO_2H(OH)-O sp^2 from ASP 493	2.571
		O sp^2 from CO_2H (OH)-O sp^2 from GLU 419	3.135
6ClPQ12	−35.34/0.07	SER 422, ALA 423, ASP 491, ASP 421, GLY 420, LYS 442, LEU 441, GLY 443, GLU 419, LYS 444, ILE 499, GLY 496, and ASP 495	
		O sp^2 from CO-O sp^3 from SER 422	2.942
		O sp^2 from CO-N sp^2 from SER 422	3.185
HPQ12	−40.45/0.13	SER 422, ALA 423, ASP 421, GLY 420, LYS 442, LEU 441, GLY 443, GLU 419, LYS 444, ILE 499, GLY 496, and ASP 495	
		O sp^2 from CO-O sp^3 from SER 422	2.993
		O sp^2 from CO-N sp^2 from SER 422	3.060
		O sp^2 from CO-N sp^2 from ASP 421	3.159

Ligand	Score/ RMSD (Å)	Group interaction/hydrogen bond	Bond length (Å)
6MePQ12	−35.39/0.17	SER 422, ALA 423, ASP 421, ASP 491, GLY 420, LYS 442, LEU 441, GLY 443, GLU 419, LYS 444, ILE 499, GLY 496, and ASP 495	
		O sp^2 from CO-O sp^3 from SER 422	2.943
		O sp^2 from CO-N sp^2 from SER 422	3.156
PQ13	−38.74/0.19	SER 422, ASP 421, ASP 4921, GLY 420, LYS 422, LEU 441, GLY 443, GLU 419, LYS 444, ILE 499, ASP 495, ARG 1029, HIS 1077, SER 1080, ASP 1079, GLY 1079, and HIS 1075	
		O sp^2 from CO-N sp^2 from ARG 1029	2.963
		O sp^2 from CO_2H (OH)-N sp^2 from ARG 1029	3.081
		O sp^2 from NO_2-O sp^2 from SER 1080	2.489
6ClPQ13	−37.47/0.32	SER 422, ALA 423, ASP 421, GLY 420, ASP 493, ASP 491, LEU 441, GLY 443, GLU 419, LYS 444, ILE 499, GLY 496, and ASP 495	
		O sp^3 from CO-O sp^3 from SER 422	2.664
		O sp^2 from CO-N sp^2 from SER 422	2.817
		O sp^2 from CO-N sp^2 from ASP 421	3.253
HPQ13	−40.08/0.05	HIS 1075, ASP 1079, CYS 1082, VAL 1041, GLY 1078, HIS 1077, SER 1080, ALA 1081, ARG 1029, LYS 444, ILE 499, ASP 495, ASP 493, GLU 419, LEU, 441, GLY 496, LYS 442, and GLY 443	
		O sp^2 from CO_2H(OH)-N sp^2 from CYS 1082	3.241
		O sp^2 from CO_2H (OH)-O sp^2 from GLY 1078	2.876
6MePQ13	−37.58/0.45	SER 422, ALA 423, ASP 421, ASP 493, ASP 491, GLY 420, LYS 442, LEU 441, GLY 443, GLU 419, LYS 444, ILE 499, and ASP 495	
		O sp^2 from CO-O sp^3 from SER 422	2.797
		O sp^2 from CO-N sp^2 from SER 422	2.926
		O sp^2 from CO-N sp^2 from ASP 421	3.247
APQ13	−42.96/0.32	SER 422, ASP 421, ASP 493, GLY 420, LYS 442, LEU 441, GLY 443, GLU 419, ILE 499, ASP 495, ILE 445, ARG 1029, and HIS 1077	
		O sp^2 from CO_2H(OH)-N sp^2 from ARG 1029	2.820
		O sp^2 from CO_2H(OH)-O sp^2 from ASP 495	3.113
		O sp^2 from CO_2H (OH)-O sp^2 from ASP 495	3.052
		N sp^3 from NH_2-O sp^2 from GLU 419	2.922
		N sp^3 from NH_2-N sp^2 from GLY 443	3.052
6ClAPQ13	−39.93/0.40	ASP 421, GLY 420, LYS 442, LEU 441, GLY 443, GLU 419, ILE 499, ILE 445, LYS 444, ASP 495, ARG 1029, and HIS 1077	
		O sp^2 from COOH(CO)-N sp^2 from ARG 1029	3.063
		O sp^2 from COOH(OH)-O sp^2 from ASP 495	3.132
		N sp^3 from NH_2-O sp^2 from GLU 419	2.706
		N sp^3 from NH_2-N sp^2 from GLY 443	3.137
HAPQ13	−37.50/0.50	HIS 1077, ARG 1029, LYS 444, ILE 445, ILE 499, ASP 495, ASP 421, GLU 419, LEU, 441, GLY 420, LYS 442, and GLY 443	
		O sp^2 from CO_2H(OH)-N sp^2 from ARG 1029	2.851
		O sp^2 from CO_2H(OH)-O sp^2 from ASP 495	3.199
		N sp^3 from NH_2-O sp^2 from GLU 419	2.707
		N sp^3 from NH_2-N sp^2 from GLY 443	3.150

Ligand	Score/ RMSD (Å)	Group interaction/hydrogen bond	Bond length (Å)
6MeAPQ13	−39.85/0.20	ASP 421, GLY 420, LYS 442, LEU 441, GLU 419, GLY 443, ILE 499, ILE 445, LYS 444, ASP 495, ARG 1029, and HIS 1077	
		O sp^2 from CO_2H(CO)-N sp^2 from ARG 1029	3.154
		O sp^2 from CO_2H(OH)-O sp^2 from ASP 495	3.115
		O sp^2 from CO_2H(OH)-O sp^2 from ASP 495	3.252
		N sp^3 from NH_2-O sp^2 from GLU 419	2.705
		N sp^3 from NH_2-N sp^2 from GLY 443	3.132

Table 4.
List of docking interactions between the ligand molecules and topoisomerase IV (PDB ID: 5EIX) from Klebsiella pneumoniae *using CLC Drug Discovery Workbench Software.*

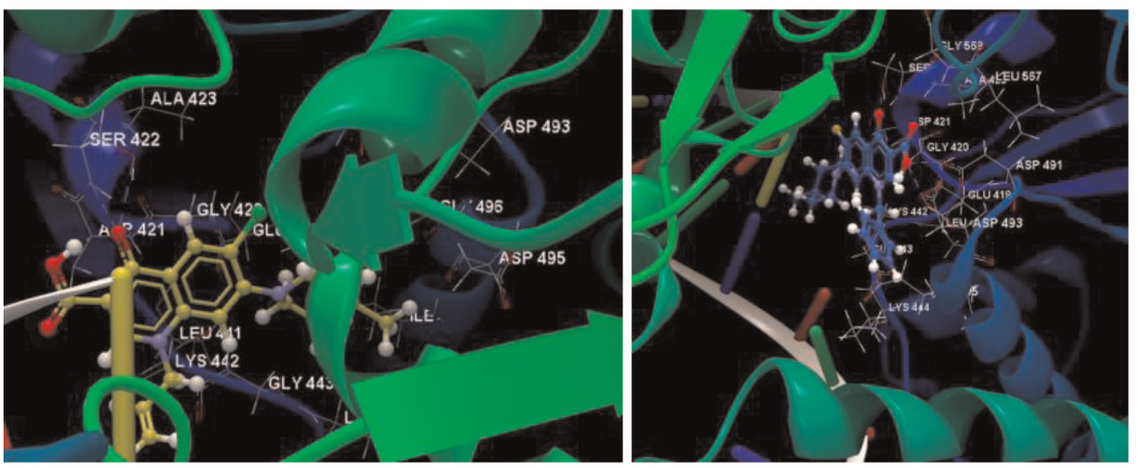

(a) (b)

Figure 13.
(a) Docking pose of 6ClPQ4 ligand interacting with amino acid residues of ligand binding site of the topoisomerase IV. (b) Docking pose of PQ11 ligand interacting with amino acid residues of ligand binding site of the topoisomerase IV.

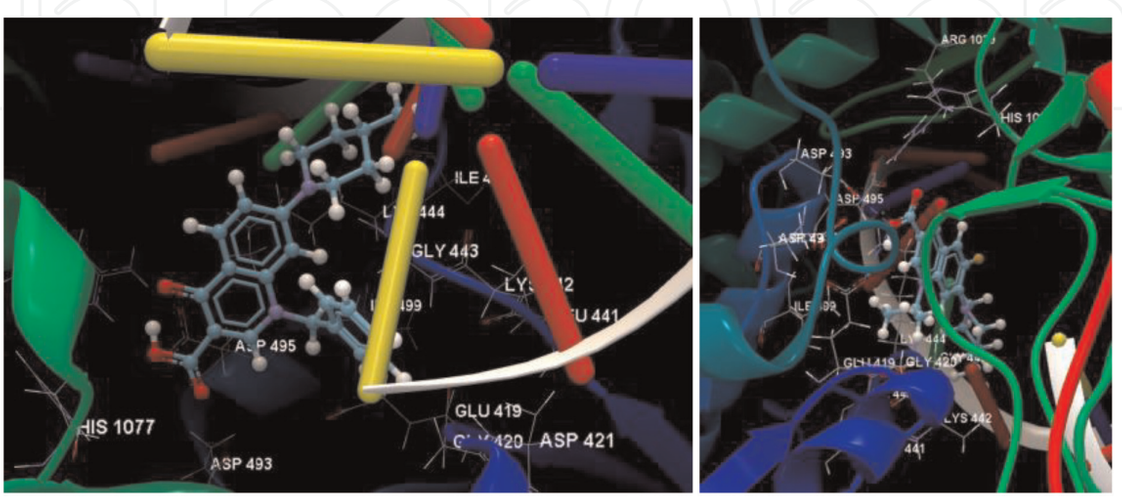

(a) (b)

Figure 14.
(a) Docking pose of HPQ11 ligand interacting with amino acid residues of ligand binding site of the topoisomerase IV. (b) Docking pose of PQ12 ligand interacting with amino acid residues of ligand binding site of the topoisomerase IV.

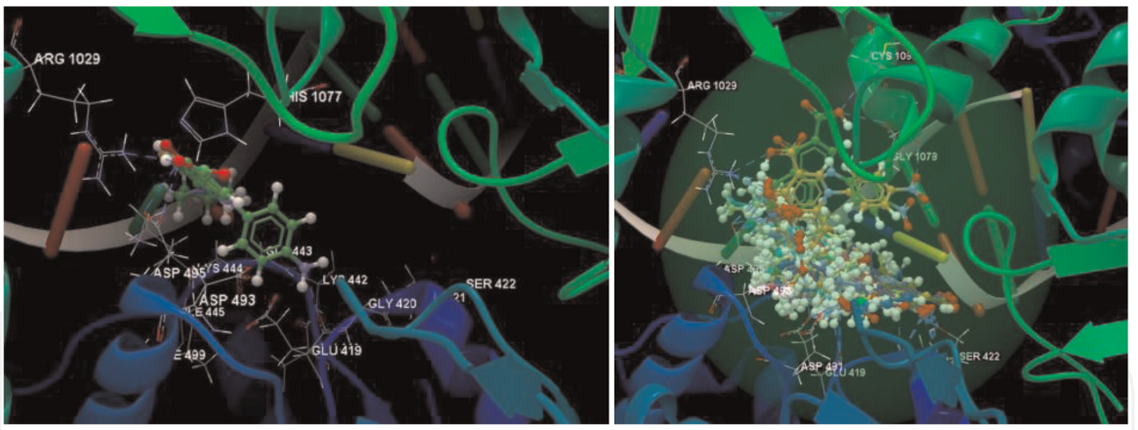

Figure 15.
(a) Docking pose of APQ13 ligand interacting with amino acid residues of ligand binding site of the topoisomerase IV. (b) Overlay of docking poses of all ligands interacting with amino acid residues of ligand binding site of the topoisomerase IV.

Ligands	Atoms	Weight (Daltons)	Flexible bonds	Lipinski violations		Hydrogen donors	Hydrogen acceptors	Log P	
				(a)	(b)			(a)	(b)
TTC	51	418.42	3	0	—	2	8	3.55	—
LFX	45	360.36	2	—	0	1	7	—	1.26
PQ4	46	344.38	4	1	1	1	5	5.34	5.67
6ClPQ4	46	360.83	4	1	1	1	5	5.87	6.20
HPQ4	46	326.39	4	1	1	1	5	5.24	5.57
6MePQ4	49	340.42	4	1	1	1	5	5.60	5.94
PQ11	52	394.44	4	1	1	1	5	5.99	6.52
6ClPQ11	52	410.89	4	1	1	1	5	6.52	7.05
HPQ11	52	376.45	4	1	1	1	5	5.89	6.42
6MePQ11	55	390.47	4	1	1	1	5	6.25	6.78
PQ12	48	346.40	3	1	1	1	5	5.10	5.63
6ClPQ12	48	362.85	3	1	1	1	5	5.63	6.16
HPQ12	48	328.41	3	0	1	1	5	5.00	5.53
6MePQ12	51	342.43	3	1	1	1	5	5.36	5.89
PQ13	51	425.41	4	1	1	1	8	6.08	6.42
6ClPQ13	51	441.86	4	1	1	1	8	6.61	6.94
HPQ13	51	407.42	4	1	1	1	8	5.98	6.31
6MePQ13	54	421.45	4	1	1	1	8	6.35	6.68
APQ13	51	395.43	3	1	1	3	6	5.37	5.90
6ClAPQ13	51	411.88	3	1	1	3	6	5.90	6.43
HAPQ13	51	377.44	3	1	1	3	6	5.27	5.80
6MeAPQ13	54	391.46	3	1	1	3	6	5.63	6.17

(a) For protein receptor PDB ID: 1K4T.
(b) For protein receptor PDB ID: 5EIX.

Table 5.
Ligands with various properties.

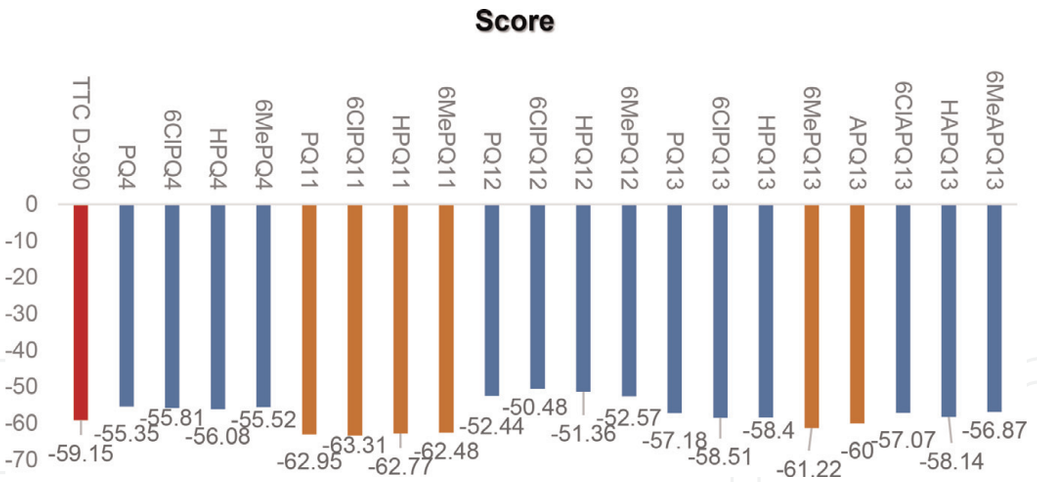

Figure 16.
Docking scores of the investigated quinolone compounds targeting human DNA topoisomerase I (PDB ID: 1K4T).

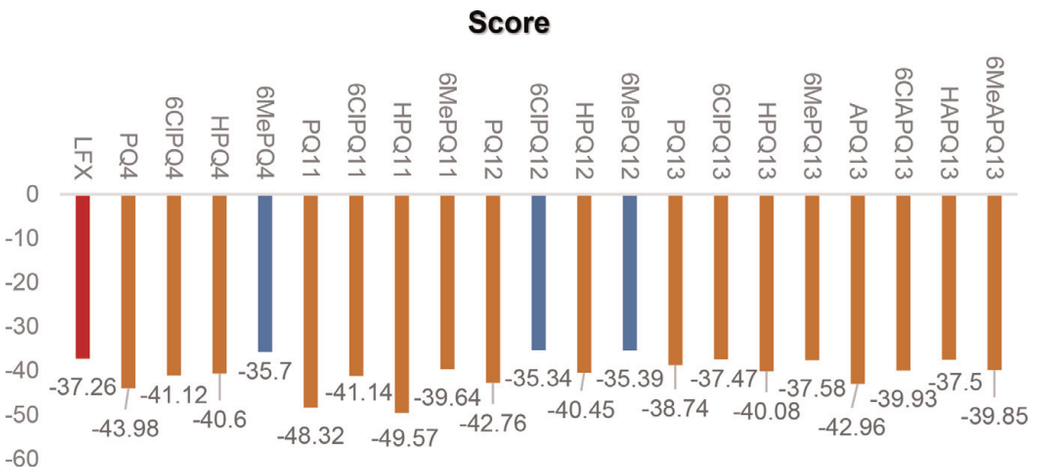

Figure 17.
Docking scores of the investigated quinolone compounds targeting topoisomerase IV (PDB ID: 5EIX) from Klebsiella pneumoniae.

pneumoniae. In case of the molecular docking studies on the human DNA topoisomerase I, all the quinolone derivatives reveal docking scores greater than −50. Only five compounds, e.g., PQ11 (−63.31), 6ClPQ11 (−62.95), HPQ11 (−62.77), 6MePQ11 (−62.48), and 6MePQ13 (−61.22), reveal better docking scores than that of co-crystallized TTC (−59.15) (**Figure 16**). In case of the molecular docking studies on topoisomerase IV from *Klebsiella pneumoniae*, only three quinolone derivatives, e.g., 6MePQ4 (−35.7), 6ClPQ12 (−35.34), and 6MePQ12 (−35.39), reveal docking scores less than that of levofloxacin (−37.26). The compounds that show better docking scores than that of levofloxacin are HPQ11 (−49.57), PQ11 (−48.32), PQ4 (−43.98), PQ12 (−42.76), APQ13 (−42.96), and 6ClPQ4 (−41.12) (**Figure 17**). It was observed that the presence of the benzyl substituent in N-1 position of the 7(4-methyl-piperidinyl)-quinolones core leads to increased docking score against human DNA topoisomerase and topoisomerase IV from *Klebsiella pneumoniae*. The compounds PQ11, 6ClPQ11, HPQ11, and 6MePQ11 reveal better docking scores than that of the reference ligands, topotecan (TTC) and levofloxacin (LFX), docked on human DNA topoisomerase (PDB ID:1K4T) and topoisomerase IV (PDB ID: 5EIX) from *Klebsiella pneumoniae*, respectively.

4. Conclusions

The virtual screening of the investigated compounds using docking has been carried out with CLC Drug Discovery Workbench Software and has led to the identification of quinolone derivatives for inhibiting the activities of topoisomerase I and topoisomerase IV. It was observed that the presence of the benzyl substituent in N1 position of the 7-(4-methyl-piperidinyl)-quinolones core leads to increased docking score against human DNA topoisomerase and topoisomerase IV from *Klebsiella pneumoniae*.

The compounds PQ11 (1-benzyl-6-fluoro-7-(4-methyl-piperidin-1-yl)-1,4-dihydro-4-oxo-quinolin-3-carboxylic acid), 6ClPQ11 (1-benzyl-6-chloro-7-(4-methyl-piperidin-1-yl)-1,4-dihydro-4-oxo-quinolin-3-carboxylic acid), HPQ11 (1-benzyl-7-(4-methyl-piperidin-1-yl)-1,4-dihydro-4-oxo-quinolin-3-carboxylic acid), and 6MePQ11 (1-benzyl-6-methyl-7-(4-methyl-piperidin-1-yl)-1,4-dihydro-4-oxo-quinolin-3-carboxylic acid) reveal better docking scores than that of the reference ligands, topotecan (TTC) and levofloxacin (LFX), docked on human DNA topoisomerase (PDB ID: 1K4T) and topoisomerase IV (PDB ID: 5EIX) from *Klebsiella pneumoniae*, respectively.

Acknowledgements

This chapter has been financed through the NUCLEU Program, which is implemented with the support of Ministry of Research and Innovation (MCI), project no. 19-41 01 02.

Conflict of interest

The authors declare no conflict of interest.

Author details

Lucia Pintilie* and Amalia Stefaniu
National Institute of Chemical-Pharmaceutical Research and Development, Bucharest, Romania

*Address all correspondence to: lucia.pintilie@gmail.com

References

[1] Pintilie L. Quinolones: Synthesis and antibacterial activity. In: Bobbarala V, editor. Antimicrobial Agents. Rijeka: Intech; 2012. pp. 255-272. DOI: 10.5772/33215

[2] Pintilie L. Quinolone compounds with activity against multidrug-resistant gram-positive microorganisms. In: Bobbarala V, editor. Concepts, Compounds and the Alternatives of Antibacterials. Rijeka: Intech; 2015. pp. 45-80. DOI: 10.5772/60948

[3] Advani RH, Hurwitz HI, Gordon MS, Ebbinghaus SW, Mendelson DS, Wakelee HA, et al. Voreloxin, a first-in-class anticancer quinolone derivative, in relapsed/refractory solid tumors: A report on two dosing schedules. Clinical Cancer Research. 2010;**16**:2167-2175. DOI: 10.1158/1078-0432.CCR-09-2236

[4] Hawtin RE, Stockett DE, Byl JAW, McDowell RS, Tan N, Michelle R, et al. Voreloxin is an anticancer quinolone derivative that intercalates DNA and poisons topoisomerase II. PLoS One. 2010;**5**:e10186. DOI: 10.1371/journal.pone.0010186

[5] Jiar X-D, Wang S, Wang M-H, Xia G-M, Liu X-J, Chai Y, et al. Synthesis and *in vitro* antitumor activity of novel naphthyridinone derivatives. Chinese Chemical Letters. 2017;**28**:235-239. DOI: 10.1016/j.cclet.2016.07.024

[6] Khalil OM, Gedawy EM, El-Malah AA, Adly ME. Novel nalidixic acid derivatives targeting topoisomerase II enzyme; design, synthesis, anticancer activity and effect on cell cycle profile. Bioorganic Chemistry. 2019;**83**:262-276. DOI: 10.1016/j.bioorg.2018.10.058

[7] Dong Y, Xu C, Zhao X, Domagala J, Drlica K. Fluoroquinolone action against mycobacteria: Effects of C-8 substituents on growth, survival, and resistance. Antimicrobial Agents and Chemotherapy. 1998;**42**:2978-2984. DOI: 10.1128/AAC.42.11.2978

[8] Aubry A, Pan XS, Fisher LM, Jarlier V, Cambau E. Mycobacterium tuberculosis DNA Gyrase: Interaction with quinolones and correlation with Antimycobacterial drug activity. Antimicrobial Agents and Chemotherapy. 2004;**48**:1281-1288. DOI: 10.1128/AAC.48.4.1281-1288.2004

[9] Kishii R, Yamaguchi Y, Takei M. *In Vitro* activities and Spectrum of the novel Fluoroquinolone Lascufloxacin (KRP-AM1977). Antimicrobial Agents and Chemotherapy. 2017;**61**:e-00120-17. DOI: 10.1128/AAC.00120-17

[10] Murata M, Kosai K, Yamauchi S, Sasaki D, Kaku N, Uno N, et al. *In Vitro* activity of Lascufloxacin against *Streptococcus pneumoniae* with mutations in the quinolone resistance-determining regions. Antimicrobial Agents and Chemotherapy. 2018;**62**:30197-30117. DOI: 10.1128/AAC.01971-17

[11] Walsh CT, Wencewicz TA. Prospects for new antibiotics: A molecule-centered perspective. The Journal of Antibiotics. 2014;**67**:7-22 https://doi.org/10.1038/ja.2013.49

[12] Flick AC, Ding HX, Leverett CA, Fink SJ, O'Donnell CJ. Synthetic approaches to new drugs approved during 2016. Journal of Medicinal Chemistry. 2018;**61**:7004-7031. DOI: 10.1021/acs.jmedchem.8b00260

[13] CLC Drug Discovery Workbench. Available from: http://www.clcbio.com

[14] Pintilie L, Oniscu C, Voiculescu G, Draghici C, Caproiu MT, Alexandru N, et al. Synthesis and antibacterial activity of some novel fluoroquinolones. Romanian Biotechnological Letters. 2003;**8**:1197-1204

[15] Pintilie L, Oniscu C, Voiculescu G, Draghici C, Caproiu MT, Alexandru N, et al. Synthesis of some novel desfluoroquinolones. Romanian Biotechnological Letters. 2003;**8**: 1303-1309

[16] Pintilie L, Oniscu C, Draghici C, Caproiu MT, Alexandru N, Damian E, et al. 6 methyl-quinolones with biological activity. Romanian Biotechnological Letters. 2003;**8**: 1163-1168

[17] Pintilie L, Negut C, Oniscu C, Caproiu MT, Nechifor M. Synthesis and antibacterial activity of some novel desfluoroquinolones. Revista de Chimie. 2009;**60**:871-975

[18] Pintilie L, Negut C, Oniscu C, Caproiu MT, Nechifor M, Iancu L, et al. Synthesis and antibacterial activity of some novel quinolones. Romanian Biotechnological Letters. 2009;**14**: 4756-4767

[19] Pintilie L, Tanase C. RO Patent application RO A/00767; 02.10.2018

[20] Pintilie L, Nita S. RO 128027-B1/ 28.02.2018

[21] Spartan'14 Wavefunction, Inc. Irvine, CA. Available from www.wavefun.com

[22] Pintilie L, Stefaniu A. Docking studies on novel analogues of 8-chloro-quinolones against *Staphylococcus aureus*. In: Vlachakis DP, editor. Molecular Docking. Rijeka: Intech; 2018. pp. 77-98. DOI: 10.5772/ intechopen.72995

[23] Staker BL, Hjerrild K, Feese MD, Behnke CA, Burgin AB Jr, Stewart L. The mechanism of topoisomerase I poisoning by a camptothecin analog. PNAS. 2002;**26**: 15387-15392. DOI: 10.1073/ pnas.242259599

[24] Veselkov DA, Laponogov I, Pan X-S, Selvarajah J, Skamrova GB, Branstrom A, et al. Structure of a quinolone-stabilized cleavage complex of topoisomerase IV from *Klebsiella pneumoniae* and comparison with a related *Streptococcus pneumoniae* complex. Acta Cryst. 2016;**D72**:488-496. DOI: 10.1107/S2059798316001212